Crystallographic fragment screening delivers diverse chemical scaffolds for Zika virus NS2B-NS3 protease inhibitor development

Xiaomin Ni[1,5], Andre Schutzer Godoy[2,5], Peter G. Marples[3,4,5] , Michael Fairhead[1,5], Blake H. Balcomb[3,4,5], Matteo P. Ferla[1,5,6], Charles W.E. Tomlinson[3,4,5], Siyi Wang[1,5], Charline Giroud[1,5], Jasmin Cara Aschenbrenner[3,4,5], Ryan M. Lithgo[3,4,5], Max Winokan[3,4,5], Anu V. Chandran[3,4,5], Warren Thompson[3,4,5], Mary-Ann Xavier[3,4,5], Eleanor P. Williams[1,5], Martin Walsh[3,4,5], Daren Fearon[3,4,5], Lizbé Koekemoer[1,5], Frank von Delft *[1,3,4,5]

1. *Centre for Medicines Discovery, Nuffield Department of Medicine Research Building, Old Road Campus, Headington, Oxford, OX3 7FZ, UK*
2. *São Carlos Institute of Physics, University of São Paulo, Av. João Dagnone, 1100 - Jardim Santa Angelina, São Carlos, 13563-120, Brazil*
3. *Diamond Light Source, Harwell Science and Innovation Campus, Fermi Ave, Didcot OX11 0DE, UK*
4. *Research Complex at Harwell, Harwell Science and Innovation Campus, Fermi Ave, Didcot, OX11 0FA, UK.*
5. ASAP Discovery Consortium: asapdiscovery.org
6. Department of Statistics, University of Oxford, 24-29 St Giles', Oxford OX1 3LB, UK

Abstract

Zika virus (ZIKV) infections cause microcephaly in new-borns and Guillain-Barre syndrome in adults raising a significant global public health concern, yet no vaccines or antiviral drugs have been developed to prevent or treat ZIKV infections. The viral protease NS3 and its co-factor NS2B are essential for the cleavage of the Zika polyprotein precursor into individual structural and non-structural proteins and is therefore an attractive drug target. Generation of a robust crystal system of co-expressed NS2B-NS3 protease has enabled us to perform a crystallographic fragment screening campaign with 1076 fragments. 48 binders with diverse chemical scaffolds were identified in the active site of the protease, with another 6 fragment hits observed in a potential allosteric binding site. Our work provides potential starting points for the development of potent NS2B-NS3 protease inhibitors. Furthermore, we have structurally characterized a potential allosteric binding pocket, identifying opportunities for allosteric inhibitor development.

Key words: co-expressed NS2B-NS3, crystallographic fragment screening, allosteric binding site

Introduction

Zika virus (ZIKV) belongs to the *Flaviviridae* family and is closely related to other flaviviruses such as Dengue virus (DENV), West Nile virus (WNV) and Yellow Fever virus (YEV). ZIKV was first identified in Uganda in 1947[1], and the first substantial outbreak in humans was reported

in Yap state in 2007[2]. Ever since it has had several major outbreaks and affected over a million people[3]. Although ZIKV infections typically manifest as mild symptoms, recent outbreaks in Brazil and French Polynesia revealed that the virus can cause microcephaly in new-borns and Guillain-Barre syndrome in adults. This alarming development has sparked significant global health concern[4-6]. Yet there is no vaccine or antiviral therapeutic available for the prevention or treatment of ZIKV infection[7].

The single-stranded positive-sense ZIKV RNA first translates to a single polyprotein precursor and is further cleaved by host protease and the viral protease NS2B-NS3 into individual functional proteins. NS3 is a serine protease with a serine, histidine and aspartate catalytic triad in the active site. Approximately 40 amino acids (aa) of NS2B function as a co-factor of NS3. These residues wrap around NS3 with the C-terminal residues forming a β-hairpin structurally contributing to the protease active site as well as participating in substrate recognition[8]. Structural studies have revealed several conformations of this unique two-component NS2B-NS3 protease, specifically a closed conformation[9], an open conformation[10, 11], and a super-open conformation[12], depending on the dynamic interactions between NS2B and NS3. In the open conformation and super-open conformation, the C-terminal portion of NS2B is disordered and locates distant from the NS3 catalytic site, resulting in an unstructured substrate binding site. These two conformations therefore have been considered as inactive forms, while the closed conformation of NS2B-NS3 with a well-structured binding pocket represents a promising targeting opportunity for antiviral development.

Two strategies have been deployed to target the NS2B-NS3 protease. The first involves the development of specific inhibitors that compete with the substrate on the active site. The second strategy focuses on non-competitive inhibitors, which target allosteric sites. Despite these efforts, neither competitive nor non-competitive inhibitors have advanced to clinical trials. Most of the reported competitive NS2B-NS3 inhibitors are limited to peptide mimics, such as macrocyclic inhibitors[13, 14]. Although these peptidomimetic inhibitors display nanomolar potency against ZIKV NS2B-NS3 protease, and some have broad spectrum antiviral activity, such as against DENV and WNV as well[15], their cellular activity and pharmacokinetic properties are poor. The natural substrate preference for a dibasic residue motif also raises challenge for competitive inhibitor development. Thus, an increasing effort has focused on developing allosteric inhibitors that block the interactions between NS2B and NS3 and lock the protease in the inactive form[16, 17]. This strategy has yielded several potent non-competitive inhibitors, including NSC135618[18], which shows antiviral activity in cellular assays. Nevertheless, the allosteric site as well as the allosteric inhibitor binding mode have not yet been properly validated due to a lack of reliable structural information.

To accelerate the development of antiviral therapeutics targeting NS2B-NS3 protease, we optimized a robust crystal system of NS2B-NS3 protease in the closed conformation and performed crystallographic fragment screening against 1076 fragments. Fragment screening identified diverse chemical scaffolds at both active site and a potential allosteric site, providing structural details of fragment engagement for the rapid follow-up compound design.

Results

Establishing a suitable crystal system for fragment screening

Several constructs have been reported to efficiently generate the ZIKV NS3 protease bound to the NS2B co-factor region. These approaches include the insertion of a glycine linker between the NS2B and NS3, as seen in the construct named gZiPro, and the co-expression of the NS2B co-factor and NS3 protease in a bicistronic vector, as demonstrated in the construct named bZiPro[9] (Figure 1A). Construct gZiPro has been commonly used for flavivirus NS2B-NS3 protease studies. However, the artificial glycine-rich linker raises concern of altering the substrate-binding behaviour[19]. Therefore, the unlinked binary NS2B-NS3 protease is preferred for studies. In addition, bZiPro succeeded in producing a closed conformation of ZIKV NS2B-NS3 structure (PDB ID: 5GPI)[9].

To produce crystals of the closed conformation of ZIKV NS2B-NS3 protease for fragment screening, we generated a modified version of the previously published PDB structure 5GPI[9]. The model of 5GPI contains 4 protein molecules in the asymmetric unit, with the NS3 N-terminal residues in one molecule binding to a neighbouring active site, making this unsuitable for crystal soaking. A further issue with this system was that in our hands when attempting to overexpress the bZipro construct we found yields to be very low. To address these issues, we generated a new construct, designated cZiPro (Figure 1A). In this construct we removed the disordered C-terminal residues of NS2B and N-terminal residues of NS3 in 5GPI structure (Figure 1A). This optimized construct, produced as a TEV cleavable GST fusion, yielded high quantities of active ZIKV NS2B-NS3 protease consistently and reproducibly produced crystals diffracting at 1.6 Å. Our NS2B-NS3 structure was determined in the P4322 space group with only one protein molecule presenting in the asymmetric unit, which is distinct from the 5GPI model, yet the superposition of both structures revealed a backbone root-mean-square deviation (RMSD) of around 0.2Å (Figure 1B). The active site in our structure was not occluded by crystal packing, and is accessible via crystal soaking, thus making it suitable for fragment screening (Figure 1C).

Fragment hit identification by crystallographic fragment screening

We used this newly established crystal system for a crystallographic fragment screening campaign against 1076 fragments using the XChem facility at Diamond Light Source. A total of 1058 datasets with resolution ranging 1.4-2.3 Å were collected. 53 fragment hits were identified from these screening efforts (Figure 1D), with 48 hits bound in the active site and 6 in a potential allosteric site (one fragment bound to both the active site and allosteric site). Diverse chemical scaffolds were identified, including benzamide, benzothiazole/ benzimidazole and piperazines based fragments. Other moieties such as amides, pyrazoles, and sulfones were also observed from hits (Supplementary table 1).

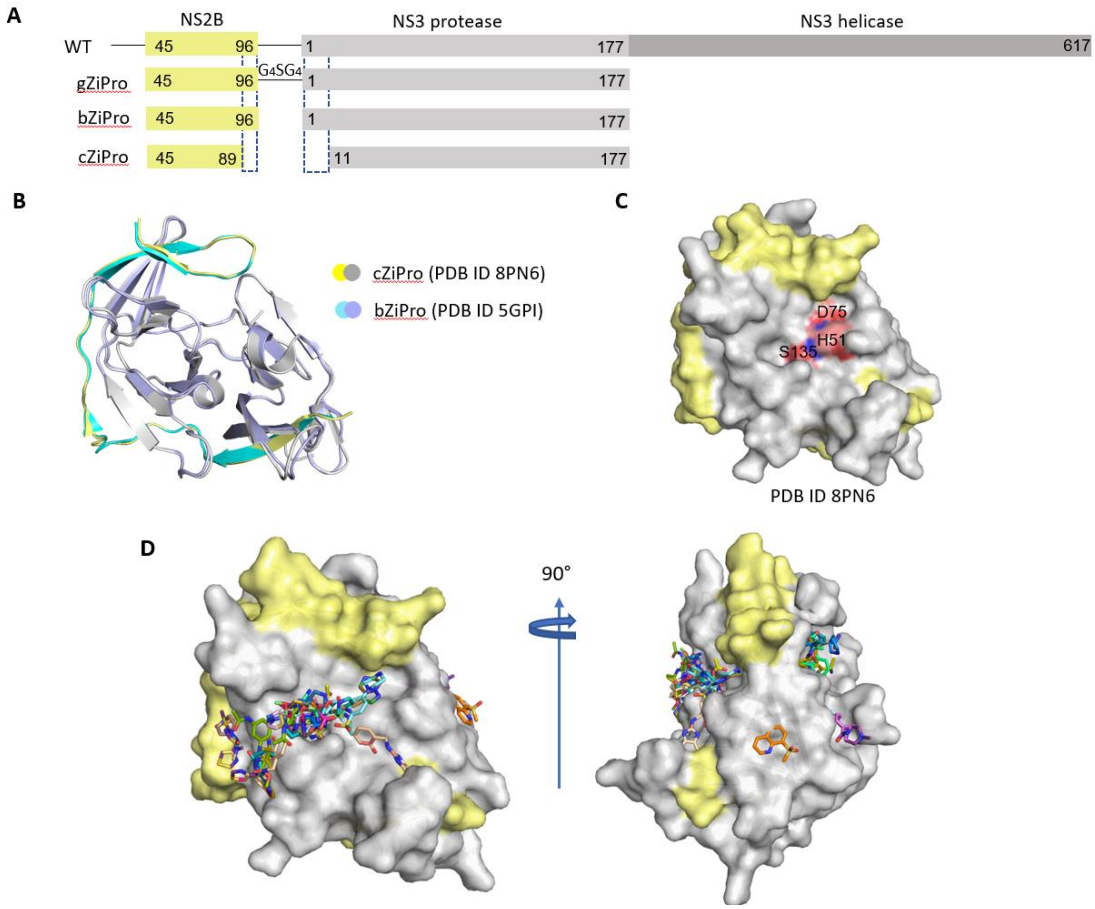

Figure1 Crystallographic fragment screening of ZIKV NS2B-NS3 protease. (A) Domain boundaries of constructs gZiPro, bZiPro and cZiPro. (B) Structure superimposition of bZiPro structure 5GPI and cZiPro structure 8PN6. (C) Surface view of apo state NS2B-NS3 protease. Catalytic site is highlighted. (D) Surface view of ZIKV NS2B-NS3 fragment screening output in two orientations. NS3 protein surface is coloured in grey and NS2B is coloured in yellow. Fragment hits are shown in sticks.

Hotspots for ligand engagement in the active site

Of the 48 fragment hits that were observed in the active site, 45 bound in the S1 site, 1 in the S1' and 2 in the S2 site, respectively (Figure 2A), suggesting S1 is a fragment binding hotspot. In the S1 site, many fragments, such as Z336080990, form π-stacking with the side chain of Tyr161. The fragment was further stabilised by three hydrogen bonds, interacting with side chain of Asp129, backbone of Tyr130, and a water, respectively (Figure 2B). Fragment Z396117078 interestingly accommodated at both S1 and S1' site (S1-S1'), forming two π-π stacking with the side chains of Tyr161 and His51. Its amide motif formed a further hydrogen bond with the backbone of Gly151 (Figure 2C). Piperazine fragment Z425338146 bound in S2 site forming a hydrogen bond with the side chain of Asp83 from NS2B, while its benzene ring formed a π-stacking interaction with His51 (Figure 2D). Analysis of the fragment-protein interactions reveals that π-stacking with the side chain of Tyr161 is a key interaction in the S1 site, represented by 39 of 48 fragment hits observed in this site (Figure 2E). Residues Asp129, Tyr130 are also observed to form hydrogen bonds with nearly a quarter of identified fragments, together with Tyr161 and Tyr150 making the S1 site as a hotspot for ligand

engagement. Besides, residue His51, Ser135 and Asn152 from NS3, plus Asp83 from NS2B were also observed in fragment interactions (Figure 2F), indicating their important role in ligand engagement.

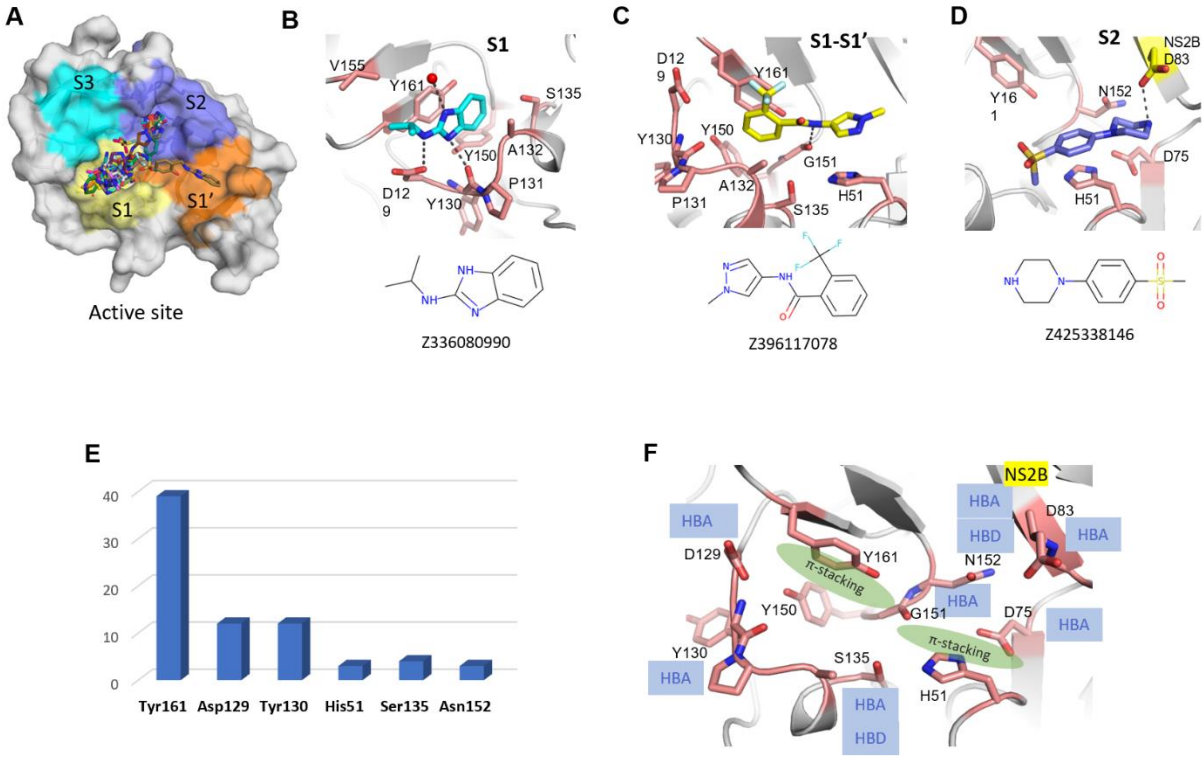

Figure2 Hotspots for ligand engagement in the active site. (A) Surface view of fragment hits bound in the active site. Examples of observed fragments Z336080990(B), Z396117078 (C) and Z425338146 (D) interacting at S1, S1-S1' and S2 site, respectively. Hydrogen bonds are shown as dashed lines. (E) Plot showing essential residues observed for fragment interaction. Y-axis represents the number of fragment hits forming interaction with associated residues. (F) Hotspots revealed from screening for ligand engagement. HBA: hydrogen bond acceptor. HBD: hydrogen bond donor.

Fragments binding to a potential allosteric site

6 fragment hits were observed outside of the orthostric site, in a pocket located beneath the catalytic residues and next to the interface between the C-terminal β-hairpin of NS2B and NS3 (Figure 3A). This potential allosteric site contains two sub-pockets, named as allosteric site 1' (AS1') and allosteric site S2' (AS2') (Figure 3A). AS1' utilizes Trp69 and Trp83 as its major interacting residues, which is defined by 2 fragments (Fragment ID: Z57122377 and Z228586974) with strong electron density. One example, Z57122377, formed π-stacking with the side chain of Trp69 and was further stabilised by hydrogen bonding to the backbone of Trp83 (Figure 3B). AS2' is formed mainly by hydrophobic residues, including Phe116, Ile123, Ala164, Ile165 from NS3, and Leu78 and Phe84 from NS2B. 4 fragments with different scaffolds were observed in AS2' in different poses. One example, Z1428159350, contains a benzene ring that formed multiple hydrophobic interactions with surrounding hydrophobic

residues, while the nitrogen atom N2 from its triazole ring formed a hydrogen bond with backbone of Gln167. Another hydrogen bond was formed between its amine group and a water molecule from solvent (Figure 3C). In contrast, Fragment Z1272515105 bound in AS2' exhibits a completely different binding mode. Its hydroxyl group formed two water-mediated hydrogen bonds with the side chains of Thr118 and Asp120 (Figure 3D). The N2 atom from its thiadiazole ring formed another water mediated hydrogen bond with Asp71, and the other nitrogen atom (N5) formed a hydrogen bond with water from solvent. Its 5-carbon ring fit in a hydrophobic cavity that formed by Ile123, Phe116 and Ala164.

In conjunction, the fragments bound in this non-active site mapped a potential allosteric pocket next to the interface of the C-terminal β-hairpin of NS2B and NS3 (Figure 3E). This observation supports previous docking and mutational studies, which proposed that allosteric site is defined by residues Gln74, Trp83, Ile123, Asn152, and Val155 (Figure 3F), and demonstrates the feasibility of allosteric inhibitor development.

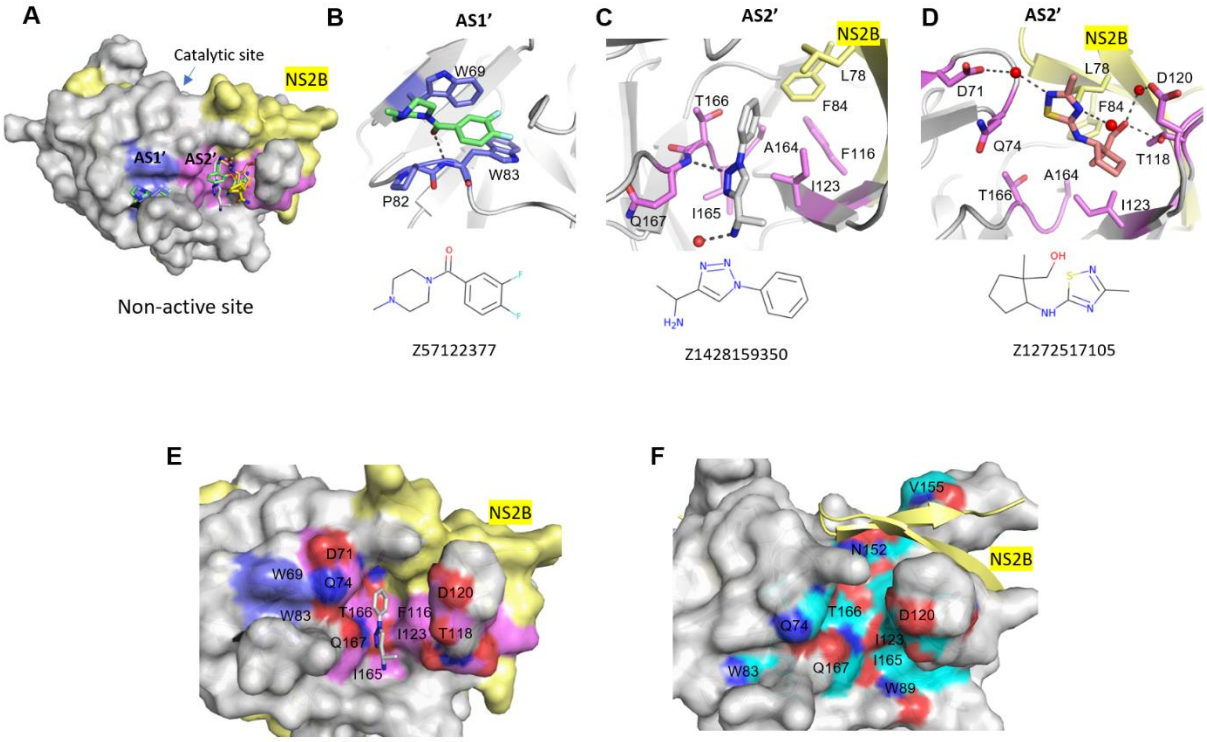

Figure3 Fragments bound in non-active site. (A) Surface view of fragments observed in the non-active site. Non-active region was coloured in blue (allosteric site 1', AS1') and pink (allosteric site 2', AS2'). (B) Structural details of observed fragment interacting at AS1'. Residues that participate in fragment interaction are shown as stick. Chemical structure of fragment is shown at bottom. Examples of fragments Z1428159350 (C) and Z1272517105 (D) bound in AS2' site. Interacting residues from NS3 are coloured in pink. Residues from NS2B forming hydrophobic pocket are coloured in yellow. Hydrogen bonds are shown as dash lines. (E) Surface view of an allosteric site defined by crystallographic fragment screening. (F) Surface view of an allosteric site defined by reported docking and mutational study.

Opportunities for rapid follow-up compound design

Our fragment screening campaign identified an interesting fragment, Z425338146, which bridges the S1 and S1' sites. The benzene ring of Z425338146 superimposed well with the benzene ring of fragment Z68299550 in the S1 site (Figure 4A), suggesting these two fragments could be merged into a single, larger scaffold (Figure 4D). In addition, Z396117078 partially overlaps with fragment Z425338146 in the S2 site (Figure 4C). Merging these two fragments would expand the small molecule to engage the S1, S1' and S2 sites simultaneously and potentially maintain the major interactions, including π-π stacking and hydrogen bonding with the protease (Figure 4E). Although biochemical and biophysical assays are required to validate whether the suggested merged molecules possess inhibitory activity against NS2B-NS3, the examples suggested here offers a potential route for rapid follow-up compound design.

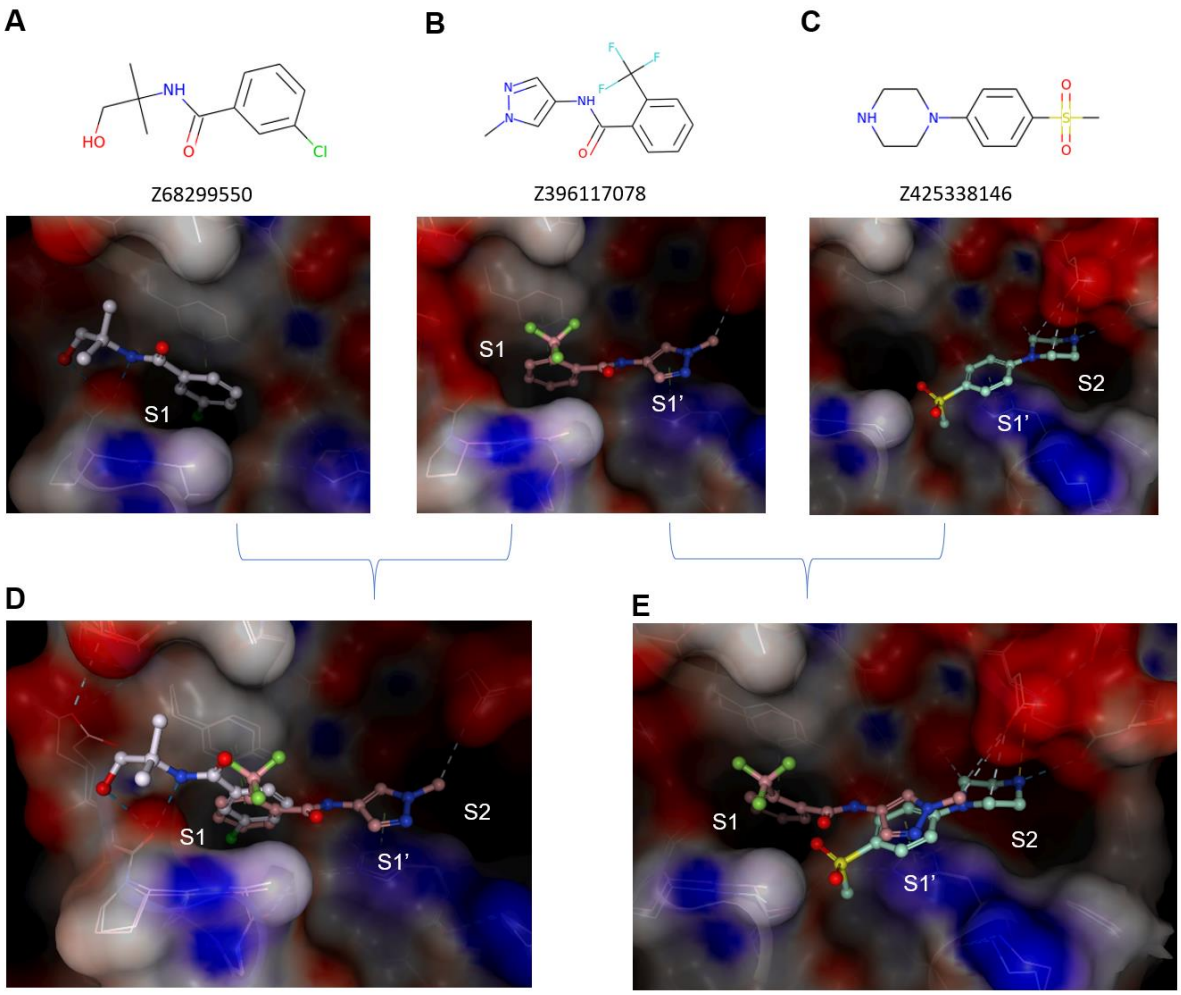

Figure4 Fragment bridging multiple sites providing opportunities for merging. Fragment Z68299550 (A) and Fragment Z396117078 (B) are partially overlapping, providing an opportunity for merging (D). Z396117078 bound to S1 and S1' site, merging with Fragment Z425338146 (C) lead to compound (E) that targets on both S1 and S2 sites.

Discussion

Similar to other flaviviruses, the NS3 protease of ZIKV requires the NS2B co-factor for stability and full activity. At the same time, ZIKV NS2B-NS3 can adopt an open, a super open, or a closed conformation, the last being ideal for inhibitor design due to well-structured binding pocket. We obtained a suitable NS2B-NS3 crystal system that applied for a successful crystallographic fragment screening, providing chemical matters for hit-to-lead development. Analysis of fragment-protein interactions reveals that Tyr161 and its surrounding residues, in particular Asp129, Tyr130, and Tyr150, as a hotspot for ligand engagement. This is supported by over 80% fragment hits being accommodated in this region. Such a high rate hits observed in S1 site is likely due to the deep pocket formed by the bulky side chains of Tyr150 and Tyr161, together with surrounding residues Tyr 130, Thr134 and Ser135. Our observation therefore highlights the S1 site as the major targeting opportunity for orthosteric inhibitor development.

The identification of several fragment hits in a potential allosteric binding site not only provides novel chemical matter for the development of potential allosteric inhibitors, but also helps to structurally characterise this putative allosteric site. Multiple allosteric sites of Flaviviral NS2B-NS3 protease have been proposed but without structural description[12, 18, 20]. Our fragment screening data presented herein, helps to reduce this knowledge gap and map the allosteric site with structural details. Although the allosteric binding pocket we described is present in a closed conformation, it is in agreement with a proposed allosteric site reported previously[12, 18], supporting the ligandability of the interface of C-terminal β-hairpin of NS2B and NS3. However, the diverse fragment scaffolds and distinct binding poses and interactions make it necessary that we acknowledge the challenges, as well as opportunities, for non-competitive inhibitor development.

Overall, our work contributes to accelerating the inhibitor development for NS2B-NS3 as well as providing a better understanding of this unique two-component NS2B-NS3 protease. In addition to describing novel chemical matter for this target and mapping the hotspots in the orthosteric site to target during hit-to-lead development, we also characterize a potential allosteric binding pocket with structural details, bringing opportunities to target alternative modes of action.

Method

Protein expression, purification and crystallization

A bicistronic construct here named cZiPro was based on the sequence of PDB model (PDB ID:5GPI). The construct was created by using a synthetic *E. coli* codon optimised gene ZIKV sequence as template (accession YP 009227202.1). Golden gate cloning was used to insert this into the pNIC-HIS6-GST-TEV-GG vector[21]. The final construct contains a GST fusion with a TEV site followed by the NS2B peptide (residues 45-89 aa). This is followed by an intervening ribosome binding site and the NS3 protease domain (residues 11-177aa). Cells cultured in TB media were initially grown at 37 °C, and they were induced with 0.5 mM IPTG at 18°C

overnight. Harvested cells were lysed by sonication in a buffer containing 50 mM HEPES, pH 7.5, 500 mM NaCl, 20 mM imidazole, 5% glycerol and 1 mM tris (2-carboxyethyl) phosphine (TCEP). The recombinant protein was initially purified by Ni2+-affinity chromatography. The His6 and GST tag was removed by TEV protease treatment, and the cleaved protein was passed through Ni2+ affinity beads and further purified by size exclusion chromatography using HPLC column in the buffer containing 25 mM HEPEs pH7.5, 150 mM NaCl, 0.5mM TCEP and 5% Glycerol. The co-expressed protein NS2B-NS3 was concentrated to ~15 mg/ml for crystallization. Crystallization was performed using sitting-drop vapor diffusion method at 20 °C. The crystals were obtained in the condition containing 30% w/v PEG2000, 0.2 M ammonium sulfate, 0.1 M sodium acetate, pH 4.8 (dx.doi.org/10.17504/protocols.io.eq2lyj51mlx9/v1)

Crystallographic fragment screening, data collection and analysis

The fragment screening was performed using the XChem facility at Diamond Light Source. The fragments from libraries of DSi-Poised Library[22], MiniFrags Probing Library[23], CovHetFrags[24], SpotXplorer[25] were dispensed into crystal drops by ECHO Liquid Handler with 20% (V/V) DMSO in the final condition and incubated for three hours at 20 °C. Crystals were harvested using Crystal Shifter [26] (Oxford Lab Technologies) and flash frozen in liquid nitrogen.

Diffraction data were collected at the I04-1 beamline at Diamond Light Source at 100 K and processed with automated pipelines using combined software, including XDS[27], Autoproc[28], Xia2[29] and DIALS[30]. All further analysis was performed using XChemExplorer[31]. Ligand restrains were generated with ACEDRG[32] and GRADE[33]. Fragment hit identification was analysed by PanDDA[34]. Electron density map was generated by Dimple[35]. Model building and refinement were carried out in COOT[36] and Buster[37] via XChemExplorer platform.

Data availablility

Crystallographic coordinate and structure factor for cZiPro crystal structure has been deposited in the PDB with the accession code 8PN6

Acknowledgement

Research reported in this publication was supported by NIAID of the National Institute of Health under award number U19AI171399. The content is solely the responsibility of the authors and does not necessarily represent the official views of the National Institute of Health. Authors acknowledge Diamond Light Source for access to the I04-1 beamline and XChem facilities through proposal lb32627.

Reference

(1) Dick, G. W.; Kitchen, S. F.; Haddow, A. J. Zika virus. I. Isolations and serological specificity. *Trans R Soc Trop Med Hyg* **1952**, *46* (5), 509-520. DOI: 10.1016/0035-9203(52)90042-4 From NLM Medline.
(2) Duffy, M. R.; Chen, T. H.; Hancock, W. T.; Powers, A. M.; Kool, J. L.; Lanciotti, R. S.; Pretrick, M.; Marfel, M.; Holzbauer, S.; Dubray, C.; et al. Zika virus outbreak on Yap Island, Federated States of Micronesia. *N Engl J Med* **2009**, *360* (24), 2536-2543. DOI: 10.1056/NEJMoa0805715 From NLM Medline.
(3) Aliota, M. T.; Bassit, L.; Bradrick, S. S.; Cox, B.; Garcia-Blanco, M. A.; Gavegnano, C.; Friedrich, T. C.; Golos, T. G.; Griffin, D. E.; Haddow, A. D.; et al. Zika in the Americas, year 2: What have we learned? What gaps remain? A report from the Global Virus Network. *Antiviral Res* **2017**, *144*, 223-246. DOI: 10.1016/j.antiviral.2017.06.001 From NLM Medline.
(4) de Araujo, T. V. B.; Ximenes, R. A. A.; Miranda-Filho, D. B.; Souza, W. V.; Montarroyos, U. R.; de Melo, A. P. L.; Valongueiro, S.; de Albuquerque, M.; Braga, C.; Filho, S. P. B.; et al. Association between microcephaly, Zika virus infection, and other risk factors in Brazil: final report of a case-control study. *Lancet Infect Dis* **2018**, *18* (3), 328-336. DOI: 10.1016/S1473-3099(17)30727-2 From NLM Medline.
(5) Krauer, F.; Riesen, M.; Reveiz, L.; Oladapo, O. T.; Martinez-Vega, R.; Porgo, T. V.; Haefliger, A.; Broutet, N. J.; Low, N.; Group, W. H. O. Z. C. W. Zika Virus Infection as a Cause of Congenital Brain Abnormalities and Guillain-Barre Syndrome: Systematic Review. *PLoS Med* **2017**, *14* (1), e1002203. DOI: 10.1371/journal.pmed.1002203 From NLM Medline.
(6) Lowe, R.; Barcellos, C.; Brasil, P.; Cruz, O. G.; Honorio, N. A.; Kuper, H.; Carvalho, M. S. The Zika Virus Epidemic in Brazil: From Discovery to Future Implications. *Int J Environ Res Public Health* **2018**, *15* (1). DOI: 10.3390/ijerph15010096 From NLM Medline.
(7) Saiz, J. C. Therapeutic Advances Against ZIKV: A Quick Response, a Long Way to Go. *Pharmaceuticals (Basel)* **2019**, *12* (3). DOI: 10.3390/ph12030127 From NLM PubMed-not-MEDLINE.
(8) Chappell, K. J.; Stoermer, M. J.; Fairlie, D. P.; Young, P. R. Insights to substrate binding and processing by West Nile Virus NS3 protease through combined modeling, protease mutagenesis, and kinetic studies. *J Biol Chem* **2006**, *281* (50), 38448-38458. DOI: 10.1074/jbc.M607641200 From NLM Medline.
(9) Zhang, Z.; Li, Y.; Loh, Y. R.; Phoo, W. W.; Hung, A. W.; Kang, C.; Luo, D. Crystal structure of unlinked NS2B-NS3 protease from Zika virus. *Science* **2016**, *354* (6319), 1597-1600. DOI: 10.1126/science.aai9309 From NLM Medline.
(10) Chen, X.; Yang, K.; Wu, C.; Chen, C.; Hu, C.; Buzovetsky, O.; Wang, Z.; Ji, X.; Xiong, Y.; Yang, H. Mechanisms of activation and inhibition of Zika virus NS2B-NS3 protease. *Cell Res* **2016**, *26* (11), 1260-1263. DOI: 10.1038/cr.2016.116 From NLM Medline.
(11) Erbel, P.; Schiering, N.; D'Arcy, A.; Renatus, M.; Kroemer, M.; Lim, S. P.; Yin, Z.; Keller, T. H.; Vasudevan, S. G.; Hommel, U. Structural basis for the activation of flaviviral NS3 proteases from dengue and West Nile virus. *Nat Struct Mol Biol* **2006**, *13* (4), 372-373. DOI: 10.1038/nsmb1073 From NLM Medline.
(12) Meewan, I.; Shiryaev, S. A.; Kattoula, J.; Huang, C. T.; Lin, V.; Chuang, C. H.; Terskikh, A. V.; Abagyan, R. Allosteric Inhibitors of Zika Virus NS2B-NS3 Protease Targeting Protease in "Super-Open" Conformation. *Viruses* **2023**, *15* (5). DOI: 10.3390/v15051106 From NLM Medline.
(13) Braun, N. J.; Quek, J. P.; Huber, S.; Kouretova, J.; Rogge, D.; Lang-Henkel, H.; Cheong, E. Z. K.; Chew, B. L. A.; Heine, A.; Luo, D.; Steinmetzer, T. Structure-Based Macrocyclization of Substrate Analogue NS2B-NS3 Protease Inhibitors of Zika, West Nile and Dengue viruses. *ChemMedChem* **2020**, *15* (15), 1439-1452. DOI: 10.1002/cmdc.202000237 From NLM Medline.
(14) Huber, S.; Braun, N. J.; Schmacke, L. C.; Quek, J. P.; Murra, R.; Bender, D.; Hildt, E.; Luo, D.; Heine, A.; Steinmetzer, T. Structure-Based Optimization and Characterization of Macrocyclic Zika Virus NS2B-NS3 Protease Inhibitors. *J Med Chem* **2022**, *65* (9), 6555-6572. DOI: 10.1021/acs.jmedchem.1c01860 From NLM Medline.
(15) Nunes, D. A. F.; Santos, F.; da Fonseca, S. T. D.; de Lima, W. G.; Nizer, W.; Ferreira, J. M. S.; de Magalhaes, J. C. NS2B-NS3 protease inhibitors as promising compounds in the development of

antivirals against Zika virus: A systematic review. *J Med Virol* **2022**, *94* (2), 442-453. DOI: 10.1002/jmv.27386 From NLM Medline.
(16) Yildiz, M.; Ghosh, S.; Bell, J. A.; Sherman, W.; Hardy, J. A. Allosteric inhibition of the NS2B-NS3 protease from dengue virus. *ACS Chem Biol* **2013**, *8* (12), 2744-2752. DOI: 10.1021/cb400612h From NLM Medline.
(17) Li, Z.; Brecher, M.; Deng, Y. Q.; Zhang, J.; Sakamuru, S.; Liu, B.; Huang, R.; Koetzner, C. A.; Allen, C. A.; Jones, S. A.; et al. Existing drugs as broad-spectrum and potent inhibitors for Zika virus by targeting NS2B-NS3 interaction. *Cell Res* **2017**, *27* (8), 1046-1064. DOI: 10.1038/cr.2017.88 From NLM Medline.
(18) Brecher, M.; Li, Z.; Liu, B.; Zhang, J.; Koetzner, C. A.; Alifarag, A.; Jones, S. A.; Lin, Q.; Kramer, L. D.; Li, H. A conformational switch high-throughput screening assay and allosteric inhibition of the flavivirus NS2B-NS3 protease. *PLoS Pathog* **2017**, *13* (5), e1006411. DOI: 10.1371/journal.ppat.1006411 From NLM Medline.
(19) Phoo, W. W.; Li, Y.; Zhang, Z. Z.; Lee, M. Y. Q.; Loh, Y. R.; Tan, Y. B.; Ng, E. Y.; Lescar, J.; Kang, C. B.; Luo, D. H. Structure of the NS2B-NS3 protease from Zika virus after self-cleavage. *Nature Communications* **2016**, *7*. DOI: ARTN 13410

10.1038/ncomms13410.
(20) Santos, N. P.; Santos, L. H.; de Magalhaes, M. T. Q.; Lei, J.; Hilgenfeld, R.; Ferreira, R. S.; Bleicher, L. Characterization of an Allosteric Pocket in Zika Virus NS2B-NS3 Protease. *J Chem Inf Model* **2022**, *62* (4), 945-957. DOI: 10.1021/acs.jcim.1c01326.
(21) Michael Fairhead; Lizbe Koekemoer; Eleanor Williams; Frank von Delft. A selection of Golden Gate vectors to simplify recombinant protein production in Escherichia coli. *BioRxiv* **2024**, PrePrint. DOI: DOI: 10.1101/2024.02.13.579886.
(22) Cox, O. B.; Krojer, T.; Collins, P.; Monteiro, O.; Talon, R.; Bradley, A.; Fedorov, O.; Amin, J.; Marsden, B. D.; Spencer, J.; et al. A poised fragment library enables rapid synthetic expansion yielding the first reported inhibitors of PHIP(2), an atypical bromodomain. *Chem Sci* **2016**, *7* (3), 2322-2330. DOI: 10.1039/c5sc03115j.
(23) O'Reilly, M.; Cleasby, A.; Davies, T. G.; Hall, R. J.; Ludlow, R. F.; Murray, C. W.; Tisi, D.; Jhoti, H. Crystallographic screening using ultra-low-molecular-weight ligands to guide drug design. *Drug Discov Today* **2019**, *24* (5), 1081-1086. DOI: 10.1016/j.drudis.2019.03.009.
(24) Keeley, A.; Abranyi-Balogh, P.; Keseru, G. M. Design and characterization of a heterocyclic electrophilic fragment library for the discovery of cysteine-targeted covalent inhibitors. *Medchemcomm* **2019**, *10* (2), 263-267. DOI: 10.1039/c8md00327k From NLM PubMed-not-MEDLINE.
(25) Bajusz, D.; Wade, W. S.; Satala, G.; Bojarski, A. J.; Ilas, J.; Ebner, J.; Grebien, F.; Papp, H.; Jakab, F.; Douangamath, A.; et al. Exploring protein hotspots by optimized fragment pharmacophores. *Nature Communications* **2021**, *12* (1). DOI: ARTN 3201

10.1038/s41467-021-23443-y.
(26) Wright, N. D.; Collins, P.; Koekemoer, L.; Krojer, T.; Talon, R.; Nelson, E.; Ye, M.; Nowak, R.; Newman, J.; Ng, J. T.; et al. The low-cost Shifter microscope stage transforms the speed and robustness of protein crystal harvesting. *Acta Crystallogr D Struct Biol* **2021**, *77* (Pt 1), 62-74. DOI: 10.1107/S2059798320014114 From NLM Medline.
(27) Kabsch, W. Xds. *Acta Crystallogr D Biol Crystallogr* **2010**, *66* (Pt 2), 125-132. DOI: 10.1107/S0907444909047337 From NLM Medline.
(28) Vonrhein, C.; Flensburg, C.; Keller, P.; Sharff, A.; Smart, O.; Paciorek, W.; Womack, T.; Bricogne, G. Data processing and analysis with the autoPROC toolbox. *Acta Crystallogr D Biol Crystallogr* **2011**, *67* (Pt 4), 293-302. DOI: 10.1107/S0907444911007773 From NLM Medline.
(29) Winter, G.: an expert system for macromolecular crystallography data reduction. *J Appl Crystallogr* **2010**, *43*, 186-190. DOI: 10.1107/S0021889809045701.
(30) Winter, G.; Waterman, D. G.; Parkhurst, J. M.; Brewster, A. S.; Gildea, R. J.; Gerstel, M.; Fuentes-Montero, L.; Vollmar, M.; Michels-Clark, T.; Young, I. D.; et al. DIALS: implementation and evaluation

of a new integration package. *Acta Crystallogr D Struct Biol* **2018**, *74* (Pt 2), 85-97. DOI: 10.1107/S2059798317017235 From NLM Medline.
(31) Krojer, T.; Talon, R.; Pearce, N.; Collins, P.; Douangamath, A.; Brandao-Neto, J.; Dias, A.; Marsden, B.; von Delft, F. The XChemExplorer graphical workflow tool for routine or large-scale protein-ligand structure determination. *Acta Crystallogr D Struct Biol* **2017**, *73* (Pt 3), 267-278. DOI: 10.1107/S2059798316020234 From NLM Medline.
(32) Long, F.; Nicholls, R. A.; Emsley, P.; Graaeulis, S.; Merkys, A.; Vaitkus, A.; Murshudov, G. N. AceDRG: a stereochemical description generator for ligands. *Acta Crystallogr D Struct Biol* **2017**, *73* (Pt 2), 112-122. DOI: 10.1107/S2059798317000067 From NLM Medline.
(33) *Smart, O. S., Womack, T. O., Sharff, A., Flensburg, C., Keller, P.,*

Paciorek, W., Vonrhein, C. and Bricogne, G. (2011). Grade, version

1.2.20. Cambridge, United Kingdom, Global Phasing Ltd.,

. (accessed.
(34) Pearce, N. M.; Krojer, T.; Bradley, A. R.; Collins, P.; Nowak, R. P.; Talon, R.; Marsden, B. D.; Kelm, S.; Shi, J.; Deane, C. M.; von Delft, F. A multi-crystal method for extracting obscured crystallographic states from conventionally uninterpretable electron density. *Nat Commun* **2017**, *8*, 15123. DOI: 10.1038/ncomms15123 From NLM PubMed-not-MEDLINE.
(35) Keegan, R.; Wojdyr, M.; Winter, G.; Ashton, A. DIMPLE: A difference map pipeline for the rapid screening of crystals on the beamline. *Acta Crystallogr A* **2015**, *71*, S18-S18. DOI: 10.1107/S2053273315099702.
(36) Emsley, P.; Lohkamp, B.; Scott, W. G.; Cowtan, K. Features and development of Coot. *Acta Crystallogr D Biol Crystallogr* **2010**, *66* (Pt 4), 486-501. DOI: 10.1107/S0907444910007493 From NLM Medline.
(37) Smart, O. S.; Womack, T. O.; Flensburg, C.; Keller, P.; Paciorek, W.; Sharff, A.; Vonrhein, C.; Bricogne, G. Exploiting structure similarity in refinement: automated NCS and target-structure restraints in BUSTER. *Acta Crystallogr D Biol Crystallogr* **2012**, *68* (Pt 4), 368-380. DOI: 10.1107/S0907444911056058 From NLM Medline.